

This journal is © The Royal Society of Chemistry 2021

ELECTRONIC SUPPLEMENTARY INFORMATION (ESI)

Effects of Carbon Nanodot Fractionation on the Performance of Sensitized Mesoporous Titania Based Photovoltaic Devices

Jeremy B. Essner, Dustin J. Boogaart, Sheila N. Baker, and Gary A. Baker*

Department of Chemistry, University of Missouri–Columbia, Columbia, MO 65211 USA.

*E-mail: bakergar@missouri.edu

Experimental

Materials and Reagents

Anhydrous citric acid (791725, $\geq 99.5\%$), urea (U5378, $\geq 98\%$), ammonium hydroxide (221228, 28.0–30.0% NH_3 basis), L-glutathione reduced (G4251, $\geq 98.0\%$), formamide (F9037, $\geq 99.5\%$), and titanium tetrachloride (208566, 99.9%) were purchased from Sigma-Aldrich (St. Louis, MO). L-arginine (BP2505500, $\geq 99\%$, free base), acetone (A949SK, $\geq 99.5\%$), isopropanol (A416, $\geq 99.5\%$), hydrochloric acid (A144S-212, 36.5–38.0%), sulfuric acid (A300S-212, 95.0–98.0 w/w%), anthracite coal (S26610), and syringe filters (09-719C, 0.20 μm pores) were acquired from Fisher Scientific (Pittsburg, PA). Ethanol (2716, 200 proof) was procured from Decon Labs (King of Prussia, PA) and regenerated cellulose dialysis membranes with molecular weight cut-offs (MWCOs) of 15 and 50 kDa (Spectra/Por® 7, 132124 and 132130, respectively) were acquired from Repligen (formerly Spectrum Labs, Rancho Dominguez, CA). All chemicals were used as received. Ultrapure Millipore water polished to a resistivity of 18.2 $\text{M}\Omega\cdot\text{cm}$ was employed for all aqueous solutions and substrate rinsing. The specific materials used for the fabrication of photovoltaic (PV) devices and their sources are provided in the ‘PV Device Preparation and Assembly’ section below.

Experimental Procedures

Four representative FCD synthetic protocols were explored in this work, specifically, a thermal pyrolysis,¹ two solvothermal syntheses,²⁻³ and a widely employed domestic microwave oven approach.⁴⁻¹⁰ Two of the employed protocols were chosen since they have been reported to result in FCDs that function as photosensitizers,¹⁻² while one of the solvothermal syntheses was reported to yield FCDs with absorption and luminescent features across the visible spectrum,³ characteristics that could prove useful in photosensitizer applications.

Thermal Treatment of Citric Acid in Aqueous Ammonium Hydroxide

N-doped FCD samples were generated following a reported protocol in which the obtained material was employed as a photosensitizer in mesoporous TiO₂-based devices.¹ Specifically, 4 g of citric acid (CA) and 1 g of ammonium hydroxide (NH₄OH) were dissolved in 10 mL of water, the mixture was transferred to a porcelain crucible, and then thermally treated at 200 °C for 3 h in a programmable oven. Upon natural cooling, the resultant carbogenic product was dispersed with 20–25 mL of acetone, the crucible was consecutively rinsed with 10- and 5-mL aliquots of acetone to collect as much product as possible, and the fractions were combined, totaling approximately 40 mL of sample. The synthesis was replicated 9–11 additional times to give a total of 10–12 individual syntheses per sample batch, which were all homogenized before proceeding. Note, substantial sedimentation was observed in the samples shortly after redispersion, therefore, once the samples were homogenized, the entire volume was allowed to sit undisturbed for 15–30 min. The acetone-dispersed supernatant was carefully decanted into 50 mL falcon tubes and centrifuged at 9k rpm for 15 min, after which, the supernatant was again carefully decanted and all sediment stemming from the reaction was discarded. Although the sediment did not disperse well in acetone and, thus, wasn't explored in this work, we note that some material appeared to disperse fairly well in water so the sediment does not consist solely of large, highly carbonized, non-polar carbon structures. After centrifugation, typically 50 mL of the supernatant, with an average concentration of 35 mg mL⁻¹, was retained for studies of the as-synthesized (as-synth.) fraction while the remaining solution volume was concentrated via rotary evaporation (25 °C, <100 mbar) to a volume of 50 mL for purification with dialysis. Initially, samples were dialyzed against water, however, as our studies progressed, substantial irreproducibility in performance was observed, which arose from apparent water-induced irreversible aggregation, as directed studies later confirmed.¹¹ Attempts were made to dialyze the samples against acetone, however, the solvent proved to be too harsh on the cellulose membranes, leading to severe membrane leakage and even complete membrane failure (*i.e.*, catastrophic rupture). We found that a mixed solvent system of 50:50 vol% acetone:ethanol worked well since the acetone content kept the material dispersed while the presence of ethanol alleviated the issues previously encountered with 100% acetone. Therefore, the concentrated supernatant fraction (40–50 mL) was dialyzed against 2 L of a 50:50 vol% acetone:ethanol mixture with a 50 kDa MWCO membrane and the dialysis solvent was refreshed daily for one week. The material permeating the membrane into the dialysis solvent over

the first 2 to 3 days of dialysis was collected, concentrated, and, eventually, dried via rotary evaporation (50 °C, <100 mbar). Once all the solvent was visibly removed, the sample was rotovaped under the same conditions for 3 h to ensure adequate removal of all ethanol and the dried material was redispersed in 50 mL of acetone to yield the dialysate (dial.) fraction. Upon completion of dialysis, the material retained within the membrane was collected and treated in a similar fashion to the dialysate fraction to yield the retentate (retent.) fraction. Solution concentrations were assessed by adding 1 mL of solution to pre-massed scintillation vials, driving off the solvent at ~65 °C, drying the material at ~80 °C for 24–48 h, and re-massing the vials to determine the mass delivered in 1 mL. All concentration assessments were conducted in triplicate and vials were massed multiple times throughout the drying period, stopping the drying once the mass values were consistent with the previous assessment. The parent solutions of the three fractions were diluted to 5, 10, or 30 mg mL⁻¹ in 100% acetone or 50:50 vol% acetone:ethanol for sensitization of TiO₂ films. Due to the poor yield of this reaction (~1% or less), the highest concentration of retentate that could be obtained that still yielded a workable volume was 5 mg mL⁻¹. Note, irreversible sedimentation was observed in as-synth. solutions of concentrations higher than 30 mg mL⁻¹, as well as the 5 mg mL⁻¹ retent. solutions.

Solvothermal Treatments of Arginine and Glutathione-Formamide

Two reported solvothermal approaches using chemically distinct precursors were explored: (i) L-arginine (Arg) and (ii) glutathione (GSH) in formamide (F). The product resulting from the former approach has been reported as a photosensitizer in mesoporous TiO₂-based devices² while the product from the latter approach is reported to exhibit strong absorbance in the visible region, particularly two distinct peaks at red wavelengths.³

(i) The Arg-derived samples were prepared by dispersing 0.35 g L-arginine in 10 mL ethanol via brief (<5 min) bath sonication and transferring the dispersion to a 23 mL Teflon-lined stainless-steel autoclave for solvothermal treatment at 200 °C for 6 h in a programmable oven. After treatment, a vibrant orange solution was obtained, which was carefully poured out and the Teflon sleeve was rinsed with a 5-mL aliquot of ethanol, combining the rinse with the orange solution. The synthesis was replicated at least nine additional times and the resulting orange solutions were homogenized to generate one sample batch. The homogenized products were placed in 50 mL

Falcon tubes and centrifuged at 9k rpm for 15 min, although, in all syntheses conducted, little to no sediment was obtained upon centrifugation. Regardless, the solutions were carefully decanted out to leave any observable sediment behind. The solutions were then homogenized again and, typically, 50 mL of this homogenized solution, with an average concentration of $\sim 18 \text{ mg mL}^{-1}$, was retained for studies of the as-synth. fraction, with approximately half of this volume being passed through a $0.2 \mu\text{m}$ syringe filter, retaining the filtrate and discarding the residue, to generate a filtered as-synth. fraction (denoted as 'as-synth. filt.'). The remaining solution volume was concentrated via rotary evaporation ($50 \text{ }^\circ\text{C}$, $<100 \text{ mbar}$) to a volume of 40 mL for purification with dialysis. Similar to the CA-NH₄OH samples, initial studies showed that the Arg-derived samples may also be negatively impacted by water (data not shown) as only a few mg of retentate was obtained even when dialyzing with a 15 kDa MWCO membrane, therefore, the samples explored in this work were dialyzed against absolute ethanol. Specifically, the concentrated samples (40–50 mL) were dialyzed against 2 L of ethanol with a 50 kDa MWCO membrane and the dialysis solvent was refreshed daily for one week. Due to the low concentrations this precursor system yields, the material permeating the membrane into the dialysis solvent was collected and concentrated via rotary evaporation ($50 \text{ }^\circ\text{C}$, $<100 \text{ mbar}$) for the entire dialysis period, although by the 4th to 5th day, very little chromophoric material appeared to still be permeating the membrane. Upon completion of dialysis, the final round of solvent was combined with the previously concentrated fractions and again concentrated via rotary evaporation ($50 \text{ }^\circ\text{C}$, $<100 \text{ mbar}$) to 50 mL to yield the dial. fraction. The parent solutions of the as-synth., as-synth. filt., and dial. fractions were diluted to 10 mg mL^{-1} in ethanol for sensitization of TiO₂ films. The original 40 mL of sample placed on dialysis was collected from the membrane and concentrated via rotary evaporation ($50 \text{ }^\circ\text{C}$, $<100 \text{ mbar}$) to 10–15 mL to yield the 10 mg mL^{-1} retent. fraction employed for sensitization of TiO₂ films. Solution concentrations were assessed in a similar fashion to the CA-NH₄OH samples. Note, irreversible sedimentation, in the form of a light orange to tan powder, was observed in all fractions days after synthesis with some electroless deposition occurring when stored in plastic Falcon tubes. Furthermore, in addition to the generation of a vibrant orange solution after the solvothermal treatment, the generation of a disc- or bean-shaped, dark red to brown solid was consistently observed in the bottom of the Teflon sleeve, whose formation was attributed to the significant quantity of L-arginine sediment in the sleeve prior to synthesis, as the L-arginine concentration of 35 mg mL^{-1} employed in the synthesis is well beyond its solubility limit in ethanol. The solid

product was sparingly soluble to insoluble in most conventional solvents, specifically, water, methanol, ethanol, isopropanol, acetone, acetonitrile, dichloromethane, dimethylformamide, dimethylsulfoxide, tetrahydrofuran, chloroform, toluene, and hexane, with higher apparent solubilities in more polar solvents. The solid pellets appeared most soluble in dimethylsulfoxide, yielding a concentration of $\sim 8 \text{ mg mL}^{-1}$. TiO_2 films were sensitized in this solution and PV characterizations were conducted, however, the performance was comparable to that of the as-synth. fraction,¹¹ therefore, the solid pellets were not explored any further. Additionally, although different concentrations of the Arg fractions were not extensively explored, a 30 mg mL^{-1} as-synth. solution was tested in devices and the increase in concentration led to a further increase in V_{OC} to over 0.6 V ,¹¹ therefore, based on the observed results, a purified retent. fraction of higher concentration may yield a doubling in performance, if the photocurrent also increases.

(ii) The GSH-F-derived samples were prepared by dissolving 100 mg of GSH in 10 mL of formamide and solvothermally treating this solution at $180 \text{ }^\circ\text{C}$ for 4 h in a 23 mL Teflon-lined stainless-steel autoclave placed in a programmable oven. After treatment and natural cooling, the viscous, greenish-black samples were collected and the sleeves were rinsed with two 5-mL aliquots of water, combining the rinses with the parent sample. The synthesis was replicated at least nine additional times and the resulting solutions were homogenized to generate one sample batch. The homogenized products were placed in 50 mL Falcon tubes and centrifuged at 9k rpm for 15 min and the supernatants were decanted into a single flask to homogenize again. Then 40–50 mL of this homogenized solution was placed on dialysis against 1.5–2 L of water with a 50 kDa MWCO membrane and the dialysis solvent was refreshed daily for one week. The remaining solution volume was set aside for as-synth. studies. The material permeating the membrane into the dialysis solvent over the first 2–3 days of dialysis was collected and concentrated via rotary evaporation ($50 \text{ }^\circ\text{C}$, $<100 \text{ mbar}$). Upon completion of dialysis, the material retained within the membrane was collected and the solution was lyophilized to obtain a solid powder. A 10 mg mL^{-1} aqueous solution of this retent. fraction was utilized for sensitization of TiO_2 . Due to the difficult-to-remove formamide content in the as-synth. and dial. fractions of this sample system, solid powders could not be obtained for these fractions, therefore, the solutions were rotovaped ($50 \text{ }^\circ\text{C}$, $<100 \text{ mbar}$) for at least 3 h to yield 100% formamide. The solutions were then diluted in half with water and the resulting 50:50 vol% formamide:water solutions were employed for sensitization of TiO_2 . Note,

irreversible sedimentation, in the form of a green to black solid, was observed in all fractions days after synthesis and extensive electroless deposition of green to black colored thin films occurred regardless if the solutions were stored in plastic Falcon tubes or glass scintillation vials.

Domestic Microwave Treatment of Citric Acid and Urea

Following a common and widely reported protocol,⁴⁻¹⁰ FCDs were synthesized from citric acid (CA) and urea (U) in a 1:3 CA:U molar ratio using a 900 W Frigidaire domestic microwave oven. Specifically, 6 g of CA and 6 g of U were dissolved in 20 mL of water in a round bottom flask (stabilized in a beaker) and the solution was treated in the microwave on the default power setting (100% power) for 5 min, forming a charred, porous product. The resultant carbonaceous material was dissolved in 50 mL of water and the round bottom flask was rinsed with two additional 50 mL aliquots of water to ensure adequate removal of all the product, homogenizing these three fractions. The homogenized solution was placed in 50 mL Falcon tubes, centrifuged at 9k rpm for 15 min, and the supernatants were decanted into a single flask to homogenize again. Then 40–50 mL of this homogenized solution was placed on dialysis against 1.5–2 L of water with a 50 kDa MWCO membrane and the dialysis solvent was refreshed daily for one week. The remaining solution volume was set aside for as-synth. studies or additional dialysis. The material permeating the membrane into the dialysis solvent over the first 24 h of dialysis was collected and concentrated via rotary evaporation (50 °C, <100 mbar) to yield the dial. fraction. Upon completion of dialysis, the material retained within the membrane was collected and this solution, as well as the as-synth. and dial. fractions, were lyophilized to obtain solid powders. Then 10 mg mL⁻¹ aqueous solutions of these fractions were prepared for sensitization of TiO₂. Note, minor irreversible sedimentation was observed in all fractions 1–2 weeks after synthesis.

Coal-derived Graphene Quantum Dots (GQDs)

Coal-derived GQDs were generated following a reported protocol.¹² Specifically, anthracite coal was coarsely crushed with a hammer and then finely pulverized with a plastic, handheld “ball mill”. Then, 325 mg of the pulverized coal was suspended in a mixture of concentrated sulfuric (60 mL) and nitric (20 mL) acids. The suspension was bath sonicated for 2 h and then heated at 100 °C under reflux and magnetic stirring (250 rpm) for 24 h. The solution was allowed to cool naturally and the product was poured over ~12 large ice cubes (~200 mL of solid ice). The reaction

flask was rinsed multiple times with water and the rinses (totaling 100 mL) were combined with the above solution. NaOH pellets were slowly added to the product solution until the pH was near 7. The neutralized solution was gravimetrically filtered (Fisherbrand filter paper, 09-801C, P5, medium porosity), however, due to the high salt concentration, salt crystallization occurred immediately upon pouring into the filter paper. Therefore, multiple pieces of filter paper were used and copious amounts of water was passed through the filter paper to ensure that nearly all the sample had been filtered. This resulted in over 1.5 L of solution so the sample was concentrated via rotary evaporation (50 °C, <100 mbar) to decrease the volume to <1 L and then 40–50 mL fractions of the sample were dialyzed for a week against 1.5 L of water using a 50 kDa MWCO membrane, refreshing the dialysis solvent daily. Due to the large sample volume, dialysis was conducted over multiple weeks to obtain a workable volume of a reasonably concentrated solution. Once a few hundred mL of the retent. fraction were collected, the solution was concentrated via rotary evaporation (50 °C, <100 mbar) to <40 mL and the sample was lyophilized to obtain a solid powder. Then a 10 mg mL⁻¹ aqueous solution of the purified GQDs was prepared for sensitization of TiO₂.

PV Device Preparation and Assembly

TEC™ 7 fluorine-doped tin oxide (FTO) coated glass was sourced from Pilkington Glass (Toledo, OH). The large glass sheets (12" x 12") were cut down to electrode size (1" x 0.670" or ~25 mm x 17 mm) with a laboratory glass cutting table (GC0101) procured from MSE Supplies (Tucson, AZ). The cut glass was then cleaned by sequentially sonicating the substrates for 60 min in a dilute solution of Alconox® detergent (0.5 wt%), an ethanolic solution of 0.1 M HCl, isopropanol, and acetone. After cleaning with detergent and ethanolic HCl, the glass was thoroughly rinsed with water and after sonication in acetone the substrates were dried upright at 50–70 °C. The substrates were then placed in a 40 mM aqueous TiCl₄ solution for 40 min at 70 °C (FTO side up), after which the treated substrates were rinsed with water and EtOH and dried upright at 50–70 °C. Transparent titania (TiO₂) paste, sourced from GreatCell Solar (MS002010) or Sigma Aldrich (791547), was applied to the FTO side of the glass via a Doctor blade approach using precut vinyl masks (~100 µm thick) to define the film area. The adhesive-backed, removable masks were cut with outer dimensions of 1" x 0.620" (or ~25 mm x 15.8 mm) and a 1 cm² (1 cm x 1 cm) centered window cut from a 12" x 48" roll of black Cricut Premium Vinyl™ - Removable using a Cricut

Explore Air™ 2 or Cricut Maker® machine. After carefully removing the masks, the films were relaxed at room temperature in the dark for 24 h and then dried in a programmable oven at 125 °C and 200 °C for 24 and 4 h, respectively. Lastly, the dried films were sintered in a muffle furnace at 525 °C for 1 h using a ramp rate of 1 °C min⁻¹. After the 1 h sintering period, the furnace was shut off and allowed to cool naturally with the films inside. The TiO₂ films were then sensitized for 2–24 h in the FCD fractions depending on the exact sample and study being conducted. Specifically, the CA-derived fractions (*i.e.*, CA-NH₄OH, CA-U) were sensitized for 2 h, the Arg fractions for 12 h, and the GSH-F fractions for 24 h. These sensitization times were chosen based on reported times in the literature¹⁻² as well as the results of 24 h uptake studies.¹¹ Absorbance spectra of bare and sensitized TiO₂ films were collected from 200 to 1100 nm on a Cary Bio 60 UV-vis spectrophotometer prior to sensitization and device assembly, respectively. Photographs of all sensitized films were also collected. Pt counter electrodes were prepared on pre-cleaned FTO-coated glass by masking off a trough with 2 layers of Scotch™ brand tape and applying Pt paste (PT-1, 006210, GreatCell Solar or 791512, Sigma Aldrich) via a Doctor blade technique. After carefully removing the tape, the films were dried at 70–100 °C for 24 h and then fired at 450 °C for 1 h in a muffle furnace. Devices were then assembled by sandwiching a non-melted DuPont Surlyn® 60 µm spacer (Meltonix 1170-60; sourced from Solaronix, Aubonne, Switzerland) between an FCD-sensitized TiO₂ photoanode and a Pt counter electrode. Prior to clamping the device shut with 1” binder clips, electrolyte containing the I⁻/I₃⁻ redox couple (Iodolyte AN-50 from Solaronix) was injected in between the electrodes. The external areas of the devices were carefully wiped down with an EtOH soaked Kimwipe™ to remove any residual electrolyte and potential light scattering contaminants.

PV Device Characterizations

Solar irradiation (1 sun or 100 mW cm⁻²) was simulated with a Newport Oriel LCS-100 Solar Simulator (94011A-ES) equipped with a Newport AM1.5G air mass filter (81088A-LCS) and calibrated with a certified Newport Oriel silicon reference cell and meter (91150V). Current-voltage data were collected with a Keithley 2400 SourceMeter™ and Oriel IV Test Station software under reverse bias from -0.20 to 0.75 V at 0.08 V s⁻¹ with a 0.5 s pre-sweep delay and 30 ms dwell time per voltage increment. Select metrics, specifically, efficiency (η), short-circuit current density (J_{SC}), open-circuit voltage (V_{OC}), and fill factor (FF), for all characterized devices

are provided in Table S1. Monochromatic light for external quantum efficiency (EQE) measurements was generated with a 300 W Xe arc lamp whose collimated irradiation was directed through 280 or 550 nm longpass filters prior to wavelength selection with a Newport CS 130 dual grating monochromator using only grating 2 (blaze: 500, grating lines: 1200). The power density at each wavelength (*i.e.*, 300–800 nm every 10 nm) was measured with a Newport power meter (1936-R) equipped with a UV silicon detector (918D-UV-OD3R). For the collection of the power density readings, the monochromator and power meter were simultaneously controlled with Newport’s TracQBasic software. The wavelength-dependent J_{SC} values were measured with the Keithley 2400 SourceMeter™ controlled by the Oriel IV Test Station software collecting 10–30 J_{SC} values at each wavelength while holding the voltage at 0 V with a 0.5 s pre-measurement delay and 1 s dwell time per data point. The collected J_{SC} values for each wavelength were averaged and the resulting photocurrent was used in the following equation to calculate the EQE at each tested wavelength (λ_x), where P_{in} is the measured power density at each of these wavelengths.

$$EQE @ \lambda_x (\%) = \frac{J_{SC} @ \lambda_x (\mu A \text{ cm}^{-2})}{P_{in} @ \lambda_x (\mu W \text{ cm}^{-2})} \times \frac{1240}{\lambda_x (nm)} \times 100$$

CA-NH₄OH Dialysate-spiked Retentate Studies

For the CA-NH₄OH dial. spiking of retent. solutions, 1 or 5 mg mL⁻¹ acetone-dispersed CA-NH₄OH retent. solutions were prepared and the solution volume was reduced by half via rotary evaporation (25 °C, <100 mbar). An appropriate volume of 10 mg mL⁻¹ acetone-dispersed CA-NH₄OH dial. solution was then added such that the final dial. concentration would be 1 mg mL⁻¹ upon diluting the sample back to its starting volume with acetone. TiO₂ films were sensitized in this solution for 2 h and were treated and characterized in a similar fashion to all other films described herein. This process was repeated to yield final dial. concentrations of 2.5, 5, 10, or 30 mg mL⁻¹ in the 1 or 5 mg mL⁻¹ retent. solutions. Note, to yield spiked dial. concentrations of 10 and 30 mg mL⁻¹, dial. stock solutions of 60 mg mL⁻¹ or higher were employed. Ethanolic solutions of the 30 mg mL⁻¹ dial.-spiked 1 or 5 mg mL⁻¹ retent. samples were also prepared and studied. These solutions were generated by reducing the volume of the aforementioned solutions by half via rotary evaporation (25 °C, <100 mbar) and replacing the removed acetone with ethanol to yield samples dispersed in 50:50 vol% acetone:ethanol.

Mass Spectrometric Analyses

For the mass spectrometric analyses, 5 mg mL⁻¹ stocks of the CA-NH₄OH and CA-U as-synth. fractions, as well as their corresponding precursor solutions, were prepared and the solutions were appropriately diluted for analysis. Mass spectrometry (MS) was performed using an Applied Biosystems Mariner orthogonal time-of-flight instrument operated under positive ion mode, employing an electrospray ion source for sample introduction. Spectra were typically acquired and averaged over a 30 second interval having a constant total ion count. The instrument was mass calibrated externally using a series of CsI adducts between 126 and 1166 *m/z*. MS data was processed using the AB Sciex Data Explorer software.

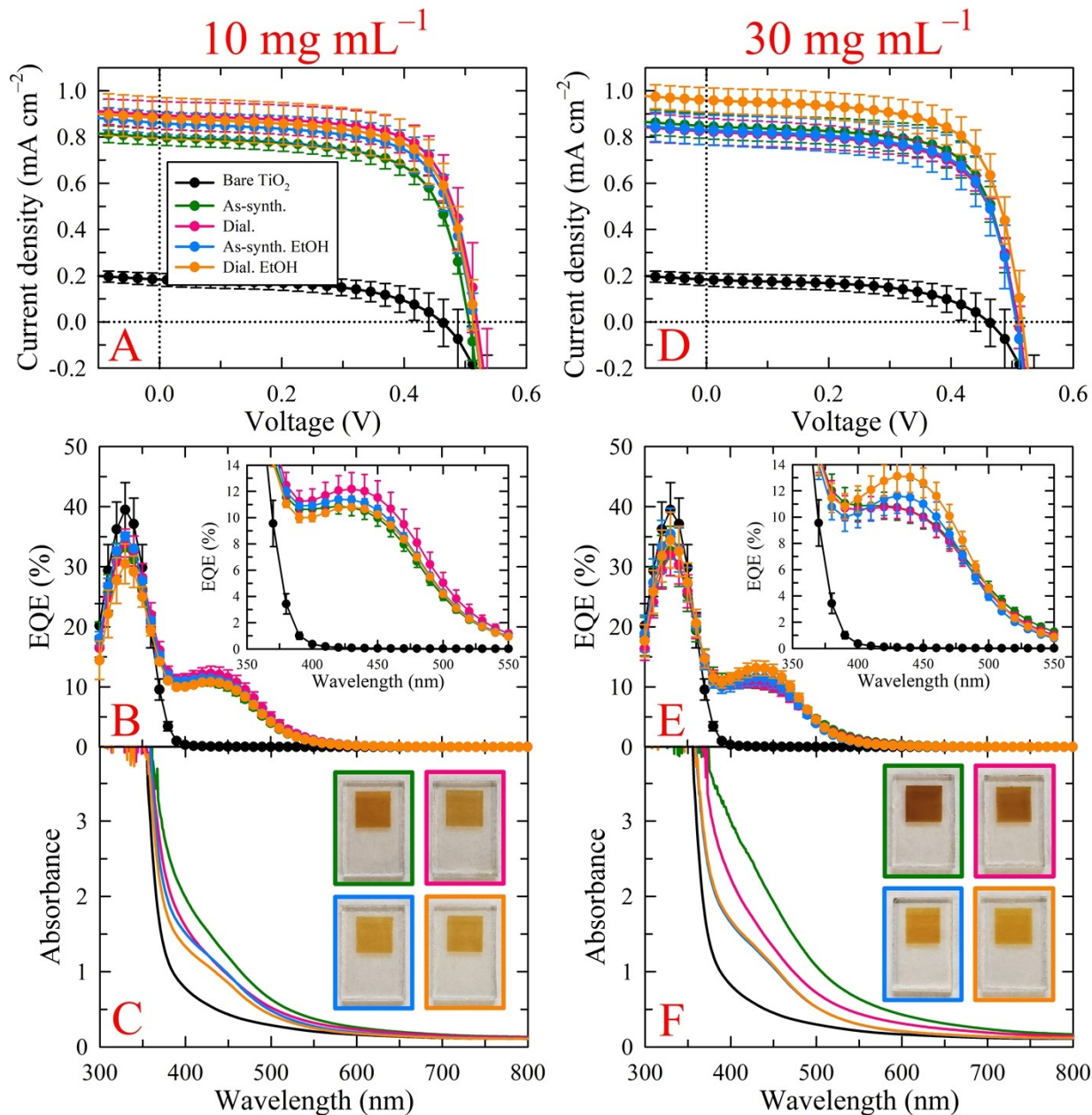


Fig. S1 Average illuminated $J-V$ curves with corresponding standard deviations for (A) 10 and (B) 30 mg mL^{-1} CA- NH_4OH -derived as-synth. and dial. fractions dispersed in 100% acetone or 50:50 vol% acetone:ethanol (denoted by “EtOH”). (B and E) Average EQE and (C and F) UV-vis absorbance spectra for these same fractions. Expanded plots of the EQE between 350 and 550 nm are provided in the insets of panels B and E. The conclusions drawn from the above results are similar to those arrived at for the 5 mg mL^{-1} as-synth. and dial. fractions; that is, device performance, mainly the photocurrent, arises from reaction by-products, specifically, species responsible for the absorbance shoulder at 450 nm and the yellow-orange color of the films. The results for bare TiO_2 (black curves) are provided in all relevant panels for comparison.

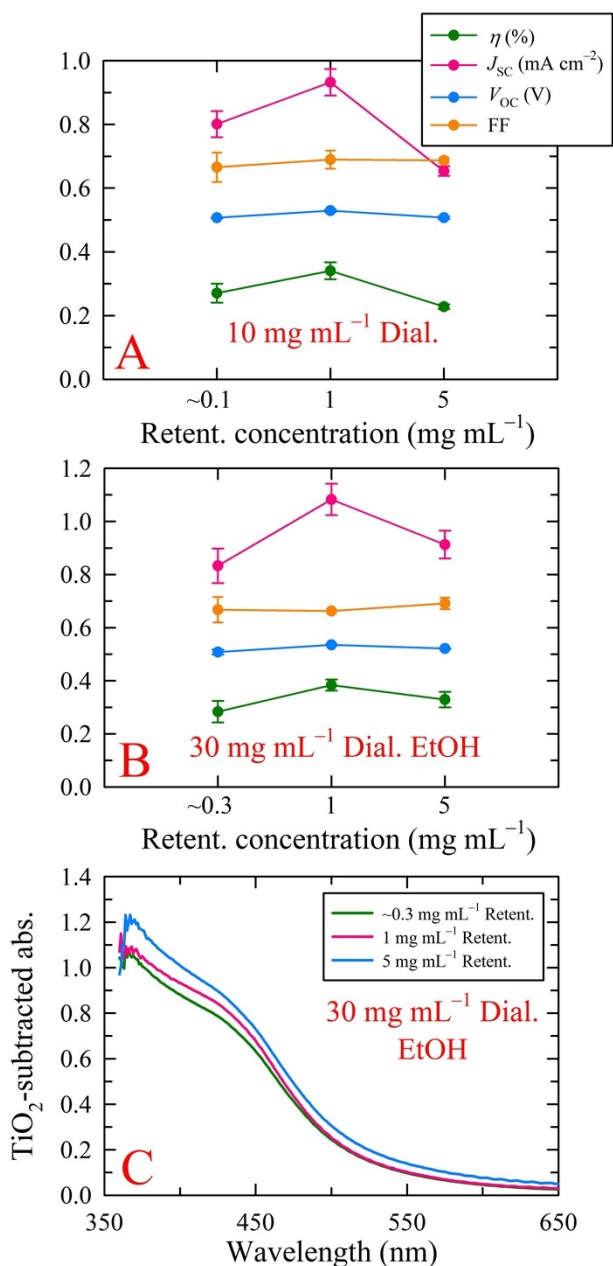


Fig. S2 Select comparisons of the spiking studies results. (A) Device metrics from the 1 and 5 mg mL⁻¹ retent. fractions spiked with dial. to a concentration of 10 mg mL⁻¹ compared to the 10 mg mL⁻¹ as-synth. fraction, which nominally contains 0.1 and 9.9 mg mL⁻¹ retent. and dial. species, respectively. (B) Device metrics from the ethanolic 1 and 5 mg mL⁻¹ retent. fractions spiked with dial. to a concentration of 30 mg mL⁻¹ compared to the ethanolic 30 mg mL⁻¹ as-synth. fraction, which nominally contains 0.3 and 29.7 mg mL⁻¹ retent. and dial. species, respectively. (C) Average UV-vis absorbance spectra for the films employed in the devices summarized in panel B. These results clearly show that synergistic effects between the dial. and retent. species exist, where an optimized nanocarbon content leads to improved device performance as widely reported in the literature. Furthermore, higher concentrations of the retent. fraction appear to diminish the apparent ‘selectivity’ observed in ethanolic solutions, evidenced by increased absorbance for higher retent. content even in the presence of 50% ethanol.

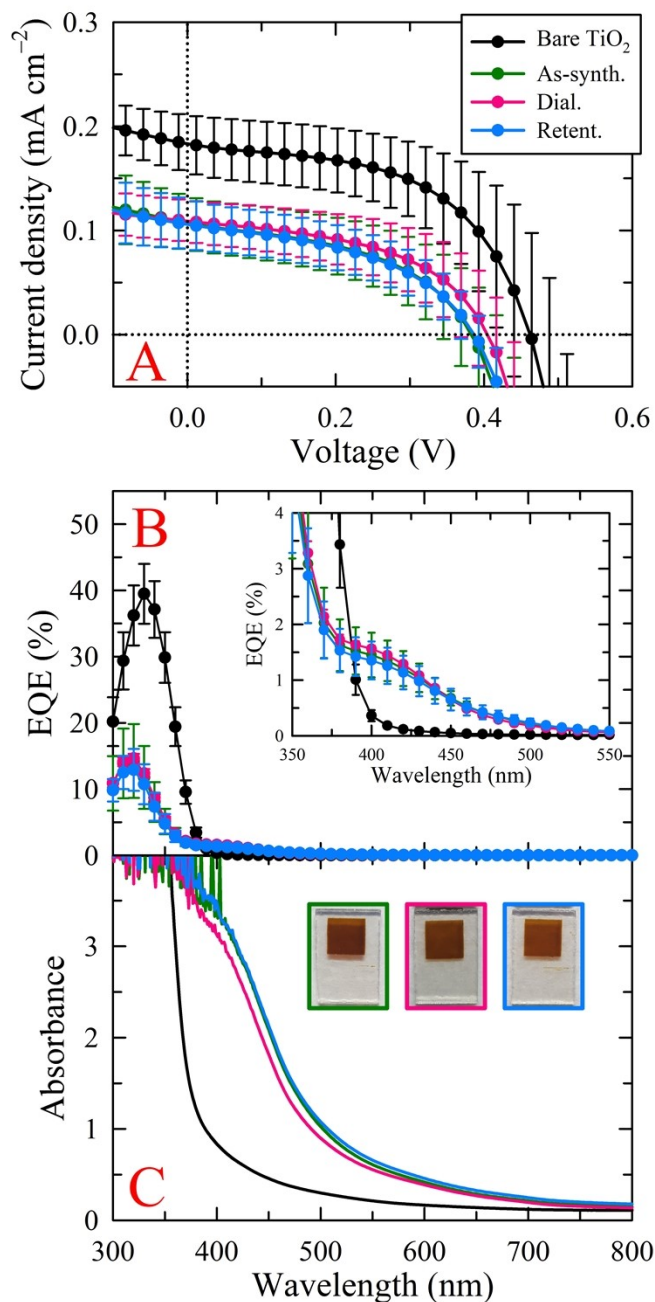


Fig. S3 (A) Average illuminated J - V curves with corresponding standard deviations of 10 mg mL⁻¹ CA-U-derived fractions dispersed in water. (B) Average EQE and (C) absorbance spectra of the three fractions. An expanded plot of the EQE between 350 and 550 nm is provided in the inset of panel B. The results for bare TiO₂ (black curves) are provided in all relevant panels for comparison. Despite the strong sensitization, all three fractions produced poorer device performance than that generated by bare TiO₂, in part, due to a massive reduction in the EQE originated from TiO₂. However, the by-products generated in this system clearly still generate photocurrent as evidenced by the observable EQE between 390 and 500 nm.

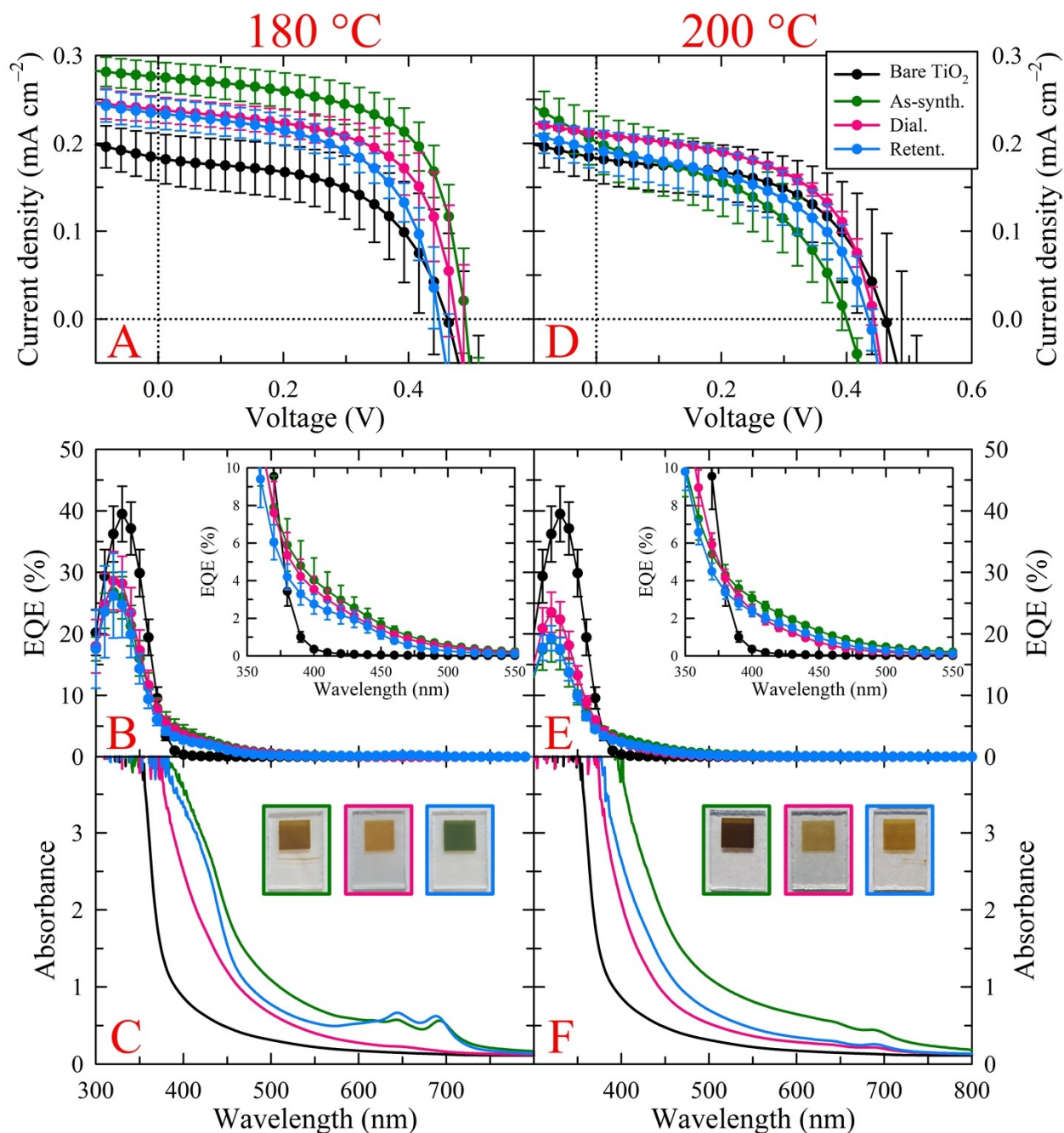


Fig. S4 Comparison of GSH-F-derived fractions synthesized at 180 and 200 °C. (A and D) Average illuminated J - V curves with corresponding standard deviations. (B and E) Average EQE and (C and F) absorbance spectra of the various fractions. Expanded plots of the EQE between 350 and 550 nm are provided in the inset of panels B and E. The results for bare TiO_2 (black curves) are provided in all relevant panels for comparison. The experimental details for these studies and an in-depth analysis of the results are provided below Fig. S5.

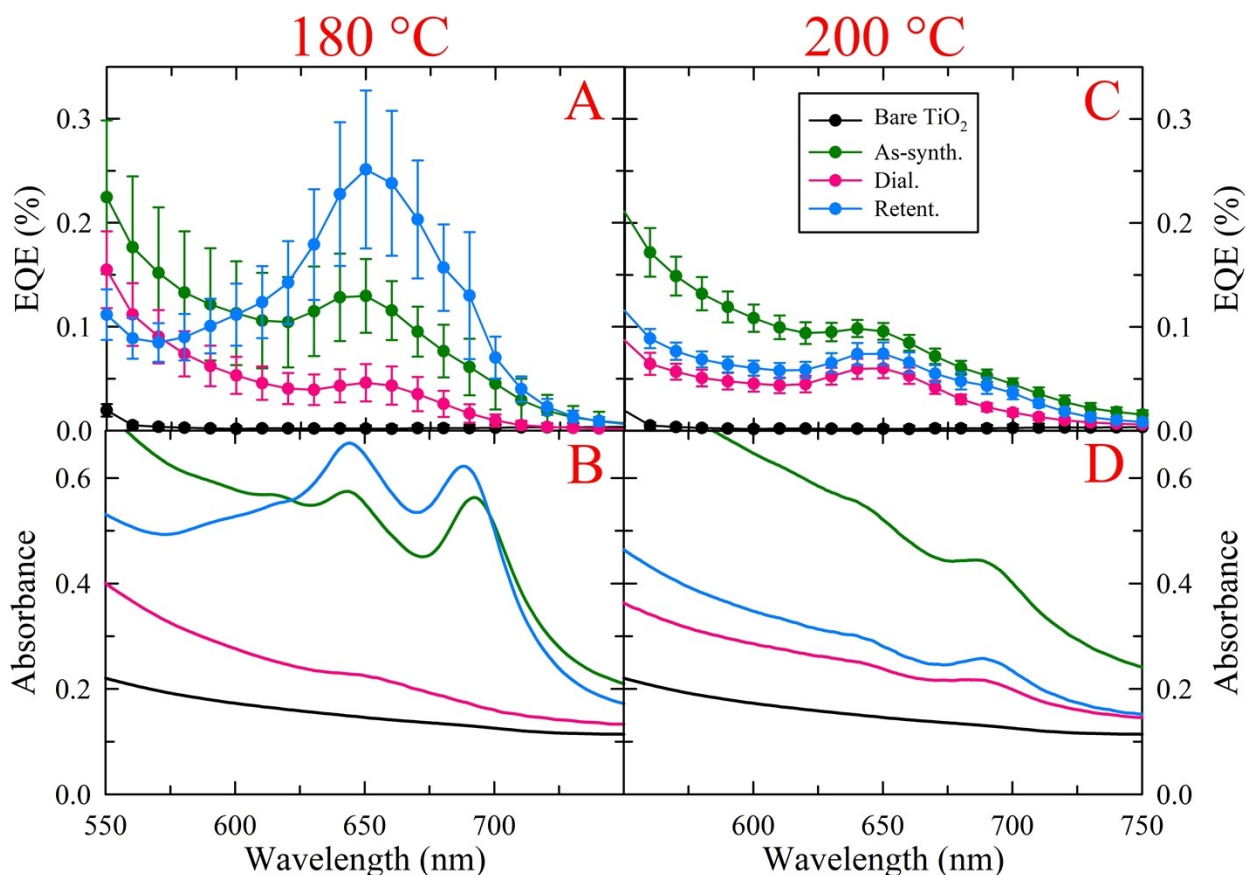


Fig. S5 Expanded plots of the (A and C) EQE and (B and D) absorbance between 550 and 750 nm for GSH-F fractions generated at synthetic temperatures of (A-B) 180 or (C-D) 200 °C.

Experimental Details and Analysis of Synthetic Temperature on GSH-F-derived Samples

All three fractions stemming from the 180 °C synthesis produced slightly higher performance than that of bare TiO₂ with the average improvement decreasing in the following order as-synth. > dial. > retent. (Fig. S4). EQE measurements revealed that these sensitizers yield photon-to-electron conversion between 375 and 550 nm with the trend in increasing EQE correlating well with the trend in J_{SC} . Additionally, akin to the CA-U system (Fig. S3), all fractions negatively impacted the EQE attributed to TiO₂ and produced a slight hypsochromic shift (~10 nm). Interestingly, the as-synth. and retent. fractions feature two minor peaks in the UV-vis spectra centered near 645 and 690 nm, which give rise to the distinct green color characteristic of this sample, particularly the retent. fraction. Indeed, upon purification of the as-synth. fraction, the solution color changed from dark brown/black with a slight green hue to a prominent dark black/green (*i.e.*, retent.), a difference that was most notable upon sensitization of the TiO₂ films, where the as-synth. fraction yielded dark brown films while the retent. fraction produced vibrant green films (Fig. S4C inset).

Interestingly, the species responsible for these absorbance features yielded minor, albeit distinguishable, photon-to-electron conversion (Fig. S5). That is, the UV-vis absorbance peak near 645 nm correlates fairly well with the EQE peak at 650 nm, however, since the UV-vis spectra display two peaks while the EQE spectra only show one, it is likely that both absorbance features contribute to the photocurrent to varying degrees such that the contributions converge into a single peak in the EQE. Although, a very minor shoulder was observed at 690 nm in the EQE spectra of the retent. fraction, a feature that directly lines up with the absorbance observed at this same wavelength. Specifically, the as-synth. fraction produced a distinct peak at 650 nm with an EQE of 0.13%, whereas, upon purification, the EQE at 650 nm for the retent. fraction promisingly jumped up to 0.25% with the EQE between 610 and 710 nm also showing an increase relative to the as-synth. fraction, a trend that correlates well with the observed changes in absorbance upon fractionation. Conversely, the dial. fraction displayed little to no peak between 620 and 720 nm with a maximum EQE of 0.05% arising at 650 nm.

Although less than 0.5%, the minor EQE peak at 650 nm observed in the GSH-F-derived retent. fraction is promising, as with a more elementary understanding of these features, the nanocarbons could be better tailored to function as efficient photosensitizers. Towards this, a second set of samples were generated at a higher carbonization temperature (200 °C instead of 180 °C) to explore any deviations in the photophysics of the species giving rise to the UV-vis and EQE spectral features between 600 and 800 nm. Other than the higher synthetic temperature, the samples and fractions were prepared and treated in the exact same manner as the 180 °C samples (see the “Solvothermal Treatments of Arginine and Glutathione-Formamide” subsection above for details). Relative to the low temperature synthesis, the average EQE observed for the as-synth. and retent. fraction at 650 nm decreased; for the latter, a substantial reduction in EQE occurred. Specifically, the EQE at this wavelength changed from 0.13 ± 0.04 , 0.25 ± 0.08 , and $0.05 \pm 0.02\%$ to 0.10 ± 0.01 , 0.07 ± 0.01 , and $0.06 \pm 0.01\%$ for the as-synth., retent., and dial. fractions, respectively. Furthermore, the EQE for these respective fractions also decreased at two select wavelengths (320 / 400 nm) from $26.75 \pm 3.26 / 4.04 \pm 1.18\%$, $26.20 \pm 6.89 / 2.75 \pm 0.52\%$, and $28.63 \pm 4.76 / 3.53 \pm 0.69\%$ to $19.10 \pm 3.67 / 3.08 \pm 0.32\%$, $19.29 \pm 2.04 / 2.37 \pm 0.28\%$, and $23.51 \pm 3.26 / 2.42 \pm 0.30\%$. Thus, the biggest effect of increasing the reaction temperature was on the EQE attributed to TiO_2 (*i.e.*, EQE at 320 nm), which indicates increased carbonization within the produced materials negatively impacts TiO_2 's photon-to-electron conversion ability. Furthermore,

the above results indicate that the higher carbonization temperature induced negative alterations to the species responsible for sensitizer-generated photocurrent, leading to diminished charge-carrier harvesting such as lower photon-to-current conversion at these redder wavelengths. We postulate that the higher reaction temperature led to the degradation of quasi-molecular moieties tethered to the nanocarbons via increased carbonization, species that are responsible for the distinct green coloration and, in part, a fraction of the photocurrent, in particular, at redder wavelengths, as evidenced by the absorbance peaks at 645 and 690 nm becoming less prominent and less distinguishable, in conjunction with the decrease in EQE in this wavelength range. Furthermore, the greater extent of carbonization brought about by a higher reaction temperature negatively impacted the other PV metrics, implying that, for this specific system, the generated nanocarbons do not function as efficient photosensitizers.

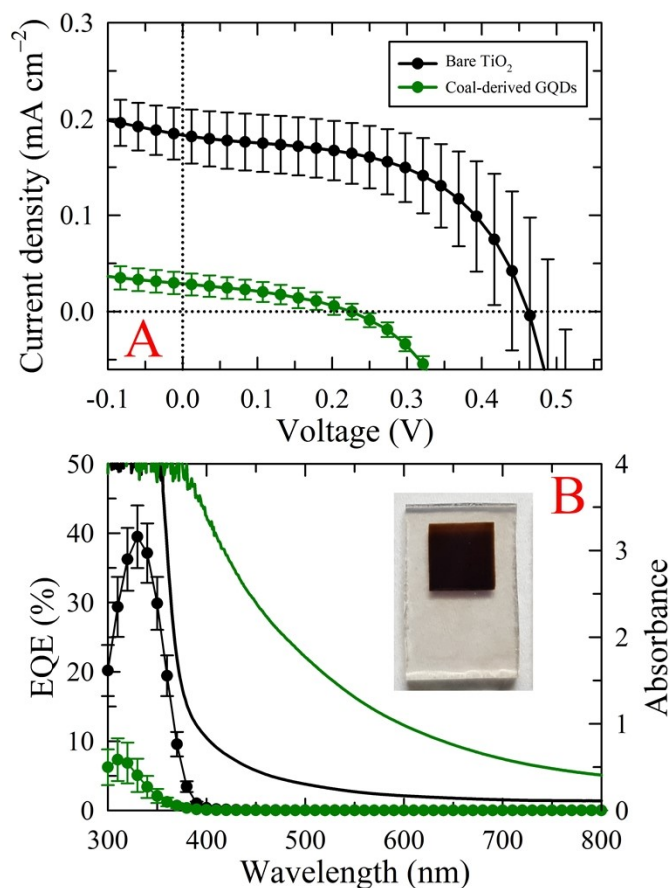


Fig. S6 Coal-derived GQDs 10 mg mL⁻¹ retent. fraction. (A) Average illuminated J - V curves with corresponding standard deviations. (B) Average EQE (left y-axis) and absorbance (right y-axis) spectra with a representative image of the sensitized TiO₂ films provided in the inset. The results for bare TiO₂ (black curves) are provided in all relevant panels for comparison. Clearly, the highly graphitic nanocarbons negatively impacted PV action, decreasing the performance well below that of bare TiO₂ and generating near-zero power conversion efficiency, despite the intense uptake or high extinction coefficient of the material. Furthermore, the graphitic nanocarbons produced essentially no photocurrent and, in fact, substantially decreased the photocurrent arising from TiO₂ and hypsochromically shifting the EQE spectrum by 20 nm.

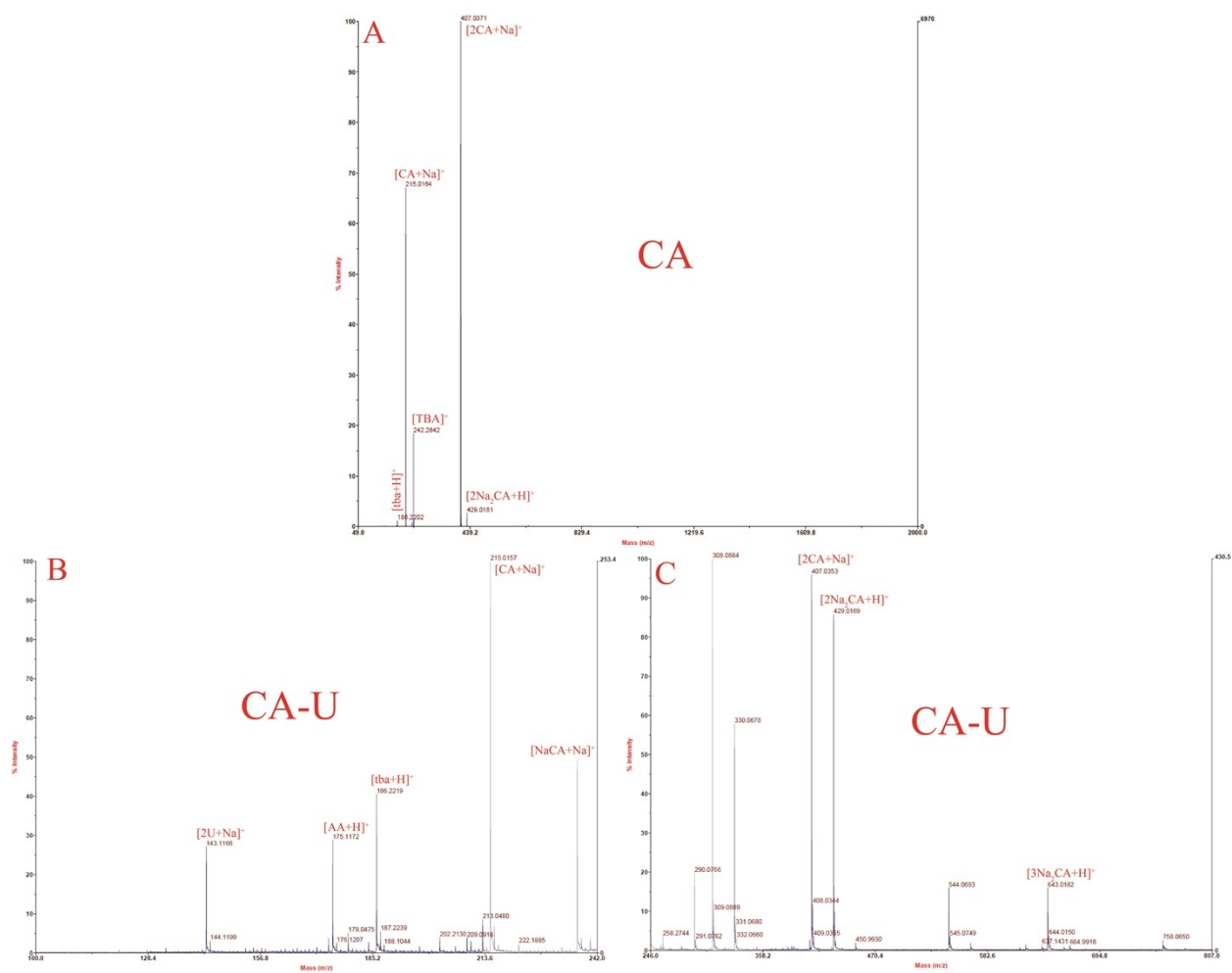


Fig. S7 Mass spectra of (A) CA and (B–C) CA-U precursor solutions from a m/z range of (A) 40–2000, (B) 100–242, and (C) 246–807.

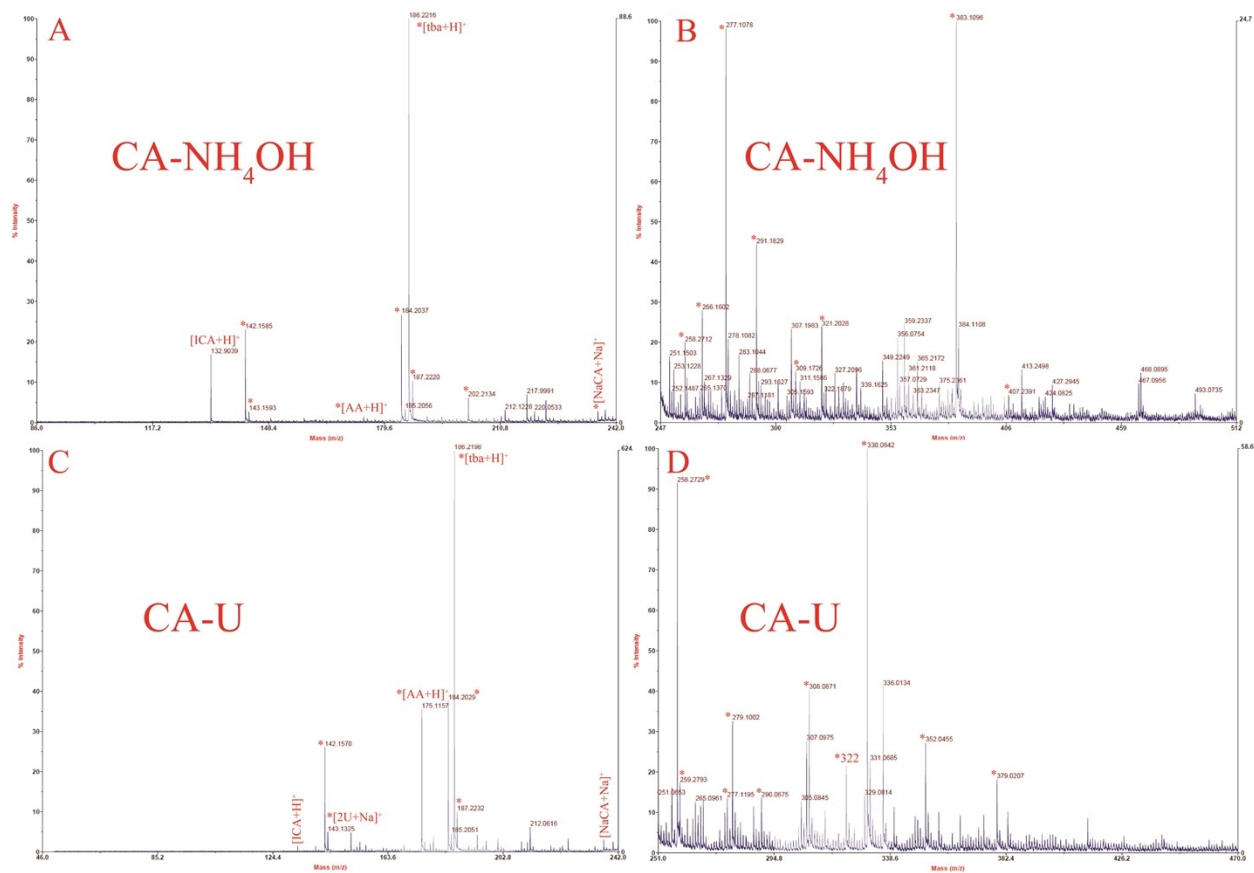


Fig. S8 Mass spectra of (A–B) CA-NH₄OH and (C–D) CA-U as-synth. fractions from *m/z* ranges of (A) 86–242, (B) 247–512, (C) 46–242, and (D) 251–470. An asterisk (*) next to a peak or peak assignment indicates that the peak was also observed in the precursor spectra.

Table S1. Photovoltaic metrics for all device sets presented in this work with 99% confidence intervals provided in parenthesis.

Precursor	Fraction	Conc. (mg mL ⁻¹)	Solvent System	Sens. Time	Device Count	η (%)	J_{sc} (mA cm ⁻²)	V_{oc} (V)	FF (%)
Bare TiO ₂	–	–	–	–	15	0.048 ± 0.015 (0.010)	0.184 ± 0.027 (0.018)	0.463 ± 0.042 (0.028)	54.8 ± 4.7 (3.1)
CA-NH ₄ OH	As-synth.	5 mg mL ⁻¹	Acetone	2 h	12	0.284 ± 0.027 (0.020)	0.827 ± 0.044 (0.032)	0.512 ± 0.007 (0.006)	67.1 ± 3.5 (2.6)
			Acetone/ EtOH		9	0.280 ± 0.030 (0.026)	0.823 ± 0.049 (0.042)	0.513 ± 0.004 (0.004)	66.3 ± 3.4 (2.9)
		10 mg mL ⁻¹	Acetone		11	0.270 ± 0.021 (0.016)	0.801 ± 0.035 (0.027)	0.507 ± 0.004 (0.003)	66.5 ± 3.5 (2.8)
			Acetone/ EtOH		4	0.301 ± 0.032 (0.042)	0.864 ± 0.049 (0.063)	0.514 ± 0.004 (0.006)	67.6 ± 3.4 (4.3)
		30 mg mL ⁻¹	Acetone		14	0.295 ± 0.032 (0.022)	0.850 ± 0.055 (0.038)	0.508 ± 0.005 (0.003)	68.2 ± 4.3 (3.0)
			Acetone/ EtOH		11	0.283 ± 0.041 (0.032)	0.833 ± 0.065 (0.050)	0.508 ± 0.009 (0.007)	66.7 ± 4.8 (3.8)
	Dial.	5 mg mL ⁻¹	Acetone	2 h	8	0.285 ± 0.035 (0.032)	0.822 ± 0.056 (0.051)	0.515 ± 0.007 (0.006)	67.1 ± 4.0 (3.7)
			Acetone/ EtOH		7	0.302 ± 0.030 (0.030)	0.862 ± 0.066 (0.065)	0.517 ± 0.008 (0.007)	67.8 ± 3.0 (2.9)
		10 mg mL ⁻¹	Acetone		8	0.323 ± 0.033 (0.030)	0.897 ± 0.059 (0.053)	0.521 ± 0.012 (0.011)	69.0 ± 2.1 (2.0)
			Acetone/ EtOH		7	0.312 ± 0.041 (0.040)	0.885 ± 0.090 (0.088)	0.516 ± 0.006 (0.006)	68.2 ± 2.4 (2.3)
		30 mg mL ⁻¹	Acetone		15	0.278 ± 0.011 (0.008)	0.826 ± 0.058 (0.039)	0.510 ± 0.006 (0.004)	66.2 ± 4.0 (2.7)
			Acetone/ EtOH		9	0.337 ± 0.034 (0.030)	0.962 ± 0.054 (0.046)	0.517 ± 0.006 (0.005)	67.5 ± 3.5 (3.0)
Retent.	1 mg mL ⁻¹	Acetone	2 h	6	0.101 ± 0.017 (0.018)	0.330 ± 0.043 (0.045)	0.471 ± 0.002 (0.002)	64.3 ± 2.9 (3.1)	
	5 mg mL ⁻¹			12	0.100 ± 0.015 (0.011)	0.317 ± 0.037 (0.028)	0.474 ± 0.011 (0.008)	66.4 ± 3.5 (2.6)	
		Acetone/ EtOH		3	0.090 ± 0.005 (0.007)	0.294 ± 0.012 (0.018)	0.473 ± 0.006 (0.009)	64.5 ± 0.9 (1.4)	

Table S1. (cont.)

Precursor	Fraction	Conc. (mg mL ⁻¹)	Solvent System	Sens. Time	Device Count	η (%)	J_{SC} (mA cm ⁻²)	V_{OC} (V)	FF (%)		
CA- NH ₄ OH	Retent. / Dial.	1 mg mL ⁻¹ / 1 mg mL ⁻¹	Acetone	2 h	3	0.141 ± 0.012 (0.018)	0.474 ± 0.031 (0.045)	0.492 ± 0.001 (0.002)	60.6 ± 2.7 (4.0)		
						0.219 ± 0.008 (0.012)	0.649 ± 0.036 (0.053)	0.517 ± 0.013 (0.020)	65.2 ± 2.7 (4.0)		
						0.264 ± 0.011 (0.016)	0.767 ± 0.064 (0.095)	0.521 ± 0.011 (0.017)	66.2 ± 1.7 (2.5)		
		1 mg mL ⁻¹ / 10 mg mL ⁻¹	Acetone/ EtOH	0.340 ± 0.027 (0.040)	0.932 ± 0.042 (0.062)	0.529 ± 0.004 (0.006)	69.0 ± 2.9 (4.2)				
		1 mg mL ⁻¹ / 30 mg mL ⁻¹		0.280 ± 0.022 (0.033)	0.812 ± 0.070 (0.105)	0.524 ± 0.003 (0.004)	65.9 ± 1.3 (2.0)				
		1 mg mL ⁻¹ / 30 mg mL ⁻¹		0.384 ± 0.021 (0.031)	1.083 ± 0.059 (0.088)	0.535 ± 0.002 (0.004)	66.3 ± 0.8 (1.2)				
		5 mg mL ⁻¹ / 1 mg mL ⁻¹	Acetone	0.079 ± 0.001 (0.001)	0.267 ± 0.005 (0.008)	0.466 ± 0.002 (0.003)	63.4 ± 0.9 (1.3)				
		5 mg mL ⁻¹ / 2.5 mg mL ⁻¹		0.122 ± 0.008 (0.012)	0.376 ± 0.019 (0.029)	0.480 ± 0.002 (0.003)	67.8 ± 1.3 (1.9)				
		5 mg mL ⁻¹ / 5 mg mL ⁻¹		0.165 ± 0.014 (0.021)	0.488 ± 0.039 (0.059)	0.492 ± 0.002 (0.003)	68.7 ± 1.5 (2.2)				
		5 mg mL ⁻¹ / 10 mg mL ⁻¹	Acetone/ EtOH	0.228 ± 0.007 (0.011)	0.653 ± 0.015 (0.023)	0.507 ± 0.004 (0.006)	68.7 ± 0.8 (1.2)				
		5 mg mL ⁻¹ / 30 mg mL ⁻¹		0.222 ± 0.012 (0.018)	0.633 ± 0.029 (0.042)	0.509 ± 0.002 (0.003)	68.7 ± 0.7 (1.1)				
		5 mg mL ⁻¹ / 30 mg mL ⁻¹		0.329 ± 0.029 (0.043)	0.913 ± 0.053 (0.078)	0.521 ± 0.001 (0.001)	69.1 ± 2.1 (3.2)				
		Arg	As-synth.	10 mg mL ⁻¹	EtOH	12 h	6	0.062 ± 0.007 (0.007)	0.190 ± 0.007 (0.007)	0.541 ± 0.008 (0.008)	59.9 ± 3.9 (4.1)
								0.055 ± 0.003 (0.004)	0.173 ± 0.005 (0.006)	0.548 ± 0.009 (0.009)	58.0 ± 1.8 (1.9)
			Dial.					0.047 ± 0.005 (0.005)	0.172 ± 0.010 (0.010)	0.472 ± 0.012 (0.013)	57.8 ± 2.1 (2.2)
Retent.	0.109 ± 0.009 (0.009)		0.297 ± 0.016 (0.017)					0.551 ± 0.005 (0.005)	66.4 ± 2.1 (2.2)		

Table S1. (cont.)

Precursor	Fraction	Conc. (mg mL ⁻¹)	Solvent System	Sens. Time	Device Count	η (%)	J_{sc} (mA cm ⁻²)	V_{oc} (V)	FF (%)						
CA-U	As-synth.	10 mg mL ⁻¹	Water	2 h	12	0.020 ± 0.009 (0.006)	0.107 ± 0.026 (0.019)	0.382 ± 0.038 (0.028)	46.8 ± 7.0 (5.2)						
						Dial.	0.025 ± 0.009 (0.007)	0.118 ± 0.025 (0.019)	0.404 ± 0.030 (0.022)	50.6 ± 6.8 (5.0)					
	Retent.					0.019 ± 0.006 (0.004)	0.106 ± 0.023 (0.017)	0.387 ± 0.020 (0.015)	45.7 ± 3.5 (2.6)						
	GSH-F					As-synth.	Unknown	Formamide/ Water	24 h	5	0.084 ± 0.011 (0.012)	0.276 ± 0.017 (0.020)	0.493 ± 0.012 (0.014)	61.6 ± 4.1 (4.7)	
											As-synth. 200 °C	3	0.035 ± 0.011 (0.016)	0.202 ± 0.031 (0.047)	0.397 ± 0.013 (0.020)
						Dial.					6	0.070 ± 0.011 (0.011)	0.240 ± 0.017 (0.018)	0.474 ± 0.022 (0.023)	61.3 ± 6.4 (6.7)
Dial. 200 °C		3	0.051 ± 0.002 (0.002)	0.212 ± 0.001 (0.002)	0.444 ± 0.004 (0.007)	54.5 ± 1.4 (2.1)									
Retent.	10 mg mL ⁻¹	Water	5	0.060 ± 0.006 (0.007)	0.235 ± 0.018 (0.020)	0.451 ± 0.013 (0.015)	56.2 ± 2.5 (2.9)								
Retent. 200 °C	3		0.041 ± 0.010 (0.015)	0.193 ± 0.023 (0.034)	0.434 ± 0.009 (0.013)	48.9 ± 4.9 (7.3)									
Coal	Retent.	10 mg mL ⁻¹	Water	24 h	4	0.002 ± 0.001 (0.002)	0.029 ± 0.012 (0.015)	0.216 ± 0.037 (0.048)	37.2 ± 1.5 (2.0)						

References

1. Wang, H.; Sun, P.; Cong, S.; Wu, J.; Gao, L.; Wang, Y.; Dai, X.; Yi, Q.; Zou, G., Nitrogen-doped Carbon Dots for “Green” Quantum Dot Solar Cells. *Nanoscale Res. Lett.* **2016**, *11* (1), 27.
2. Marinovic, A.; Kiat, L. S.; Dunn, S.; Titirici, M.-M.; Briscoe, J., Carbon-nanodot Solar Cells from Renewable Precursors. *ChemSusChem* **2017**, *10* (5), 1004–1013.
3. Wang, Y.; Lao, S.; Ding, W.; Zhang, Z.; Liu, S., A Novel Ratiometric Fluorescent Probe for Detection of Iron Ions and Zinc Ions based on Dual-emission Carbon Dots. *Sens. Actuators B Chem.* **2019**, *284*, 186–192.
4. He, L.; Wang, T.; An, J.; Li, X.; Zhang, L.; Li, L.; Li, G.; Wu, X.; Su, Z.; Wang, C., Carbon Nanodots@Zeolitic Imidazolate Framework-8 Nanoparticles for Simultaneous pH-responsive Drug Delivery and Fluorescence Imaging. *CrystEngComm* **2014**, *16* (16), 3259–3263.
5. Karthik, S.; Saha, B.; Ghosh, S. K.; Pradeep Singh, N. D., Photoresponsive Quinoline Tethered Fluorescent Carbon Dots for Regulated Anticancer Drug Delivery. *Chem. Commun.* **2013**, *49* (89), 10471–10473.
6. Niu, Q.; Gao, K.; Lin, Z.; Wu, W., Amine-capped Carbon Dots as a Nanosensor for Sensitive and Selective Detection of Picric Acid in Aqueous Solution via Electrostatic Interaction. *Anal. Methods* **2013**, *5* (21), 6228–6233.
7. Strauss, V.; Margraf, J. T.; Dolle, C.; Butz, B.; Nacken, T. J.; Walter, J.; Bauer, W.; Peukert, W.; Spiecker, E.; Clark, T.; Guldi, D. M., Carbon Nanodots: Toward a Comprehensive Understanding of their Photoluminescence. *J. Am. Chem. Soc.* **2014**, *136* (49), 17308–17316.
8. Wang, L.; Zhu, S.-J.; Wang, H.-Y.; Qu, S.-N.; Zhang, Y.-L.; Zhang, J.-H.; Chen, Q.-D.; Xu, H.-L.; Han, W.; Yang, B.; Sun, H.-B., Common Origin of Green Luminescence in Carbon Nanodots and Graphene Quantum Dots. *ACS Nano* **2014**, *8* (3), 2541–2547.
9. Qu, S.; Wang, X.; Lu, Q.; Liu, X.; Wang, L., A Biocompatible Fluorescent Ink based on Water-soluble Luminescent Carbon Nanodots. *Angew. Chem. Int. Ed.* **2012**, *51* (49), 12215–12218.
10. Qu, S.; Chen, H.; Zheng, X.; Cao, J.; Liu, X., Ratiometric Fluorescent Nanosensor based on Water Soluble Carbon Nanodots with Multiple Sensing Capacities. *Nanoscale* **2013**, *5* (12), 5514–5518.
11. Essner, J. An Evaluation of the need for Critically Refined Purification Procedures in Fluorescent Carbon Dot Syntheses: The Ramifications of the Ubiquitous Presence of Reaction By-Products on Quenchometric and Light Harvesting Applications. Dissertation, University of Missouri-Columbia, 2021.
12. Ye, R.; Xiang, C.; Lin, J.; Peng, Z.; Huang, K.; Yan, Z.; Cook, N. P.; Samuel, E. L. G.; Hwang, C.-C.; Ruan, G.; Ceriotti, G.; Raji, A.-R. O.; Martí, A. A.; Tour, J. M., Coal as an Abundant Source of Graphene Quantum Dots. *Nat. Commun.* **2013**, *4*, 2943.